Journal of
Materials Chemistry C

Materials for optical, magnetic and electronic devices

## Accepted Manuscript

This article can be cited before page numbers have been issued, to do this please use: W. Li, X. jin, Y. Zheng, X. Chang, W. Wang, T. Lin, F. Zheng, O. Onyilagha and Z. Zhu, *J. Mater. Chem. C*, 2020, DOI: 10.1039/D0TC00443J.

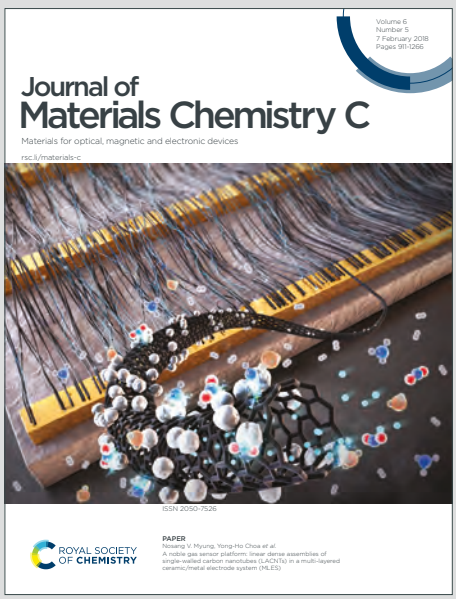




ROYAL SOCIETY OF CHEMISTRY

rsc.li/materials-c

View Article Online
DOI: 10.1039/D0TC00443J

ARTICLE

# Porous and Air Gap Elastomeric Dielectric Layer for Wearable Capacitive Pressure Sensor with High Sensitivity and Wide Detection Range

Received 00th January 20xx,
Accepted 00th January 20xx

DOI: 10.1039/x0xx00000x

Wei Li,[a,†] Xin Jin,[b,†] Yide Zheng,[a] Xudong Chang,[a] Wenyu Wang,*[a] Tong Lin,[c] Fan Zheng,[d] Obiora Onyilagh,[d] Zhengtao Zhu*[d]

Flexible and highly sensitive capacitive sensor capable of detecting the pressure over a wide range was prepared using an elastomeric dielectric layer with high porosity and air gaps sanwiched between the conducting polymer/filter paper electrodes. Porous polydimethylsiloxane (PDMS) with air gaps (i.e. through holes) was prepared by using NaCl powders and array of metal pins as template during the curing process. Capacitive sensor based on the PDMS layer with ~60% porosity and array of 6 × 6 air gaps of diameter of ~850 μm showed high sensitivity for pressure range from ~5 Pa to 1 MPa, quick response time, and good durability. The applications of the capacitive pressure sensor in human motion monitoring and spatial pressure mapping were demonstrated.

## 1. Introduction

Flexible pressure sensor is one of the key components in future human machine interface,[1, 2] human motion monitoring,[3, 4] electronic skin (E-skin),[5, 6] soft robotics, etc.[7, 8] Based on the transduction mechanism, pressure sensor can be classified as piezoresistive,[9-12] capacitive,[13, 14] piezoelectric,[15, 16] or triboelectric device.[17, 18] Among these electric transduction mechanisms, piezoresistive and capacitive sensors have been studied extensively for flexible and wearable sensors.[19, 20] Piezoresistive sensor detects external force/pressure by measuring change of the resistance from the active materials or the contacts of the device. Piezoresistive sensor is sensitive and readily integrated with electric circuity. Major drawbacks are drifting of the resistance with temperature/humidity variation and complex process for preparation of soft and conductive materials. The capacitive pressure sensor composes of a deformable dielectric material sandwiched between two flexible conductive electrodes. The change of the thickness/area of the dielectric layer under pressure results in the capacitance change sensitive to applied pressure. Capacitive pressure sensor, with advantages of low power consumption, simple device fabrication, temperature independence, etc, has been explored for wearable human motion monitoring.[21-24] Several challenges remain to further advance the capacitive sensors for flexible and wearable applications.

Human motion involves various movements over a wide range of pressure or strain. Activities such as breathing, heartbeat, etc. require detection of the low pressure from ~1 Pa to 1 kPa, whereas walking and running have pressure range from 10 to ~100 kPa. The challenges to use flexible capacitive sensor for wearable human motion monitoring include the low sensitivity and limited detection range. For example, polydimethylsiloxane (PDMS) has been the elastomer of choice for flexible capacitive sensor due to its good flexibility and elasticity. However, PDMS has a modulus of ~ 1 MPa, and therefore, the small deformation of PDMS under pressure limits the sensitivity range of the PDMS-based capacitive sensor. To expand the detection range of pressure and improve the sensitivity in the capacitive sensor, different material design strategies have been investigated.

To improve the sensitivity of the flexible capacitive sensor under small pressure, dielectric and electrode materials with microstructures of different shapes (such as pyramids,[25-27], pillars,[13, 28] or porous netting[29]) have been designed.[6, 7, 27, 30-32] The pores (air voids) formed by the microstructures in the dielectric layer can deform readily, leading to high sensitivity under small applied pressure. For example, Yang et al.[32] fabricated a porous pyramid PDMS dielectric layer by replica molding with a polystyrene coated silicon mold. The capacitive sensor based on the porous pyramid PDMS showed unprecedented sensitivity (44.5 $kPa^{-1}$) for the pressure smaller than 100 Pa. The pyramid architecture could concentrate the stress at the apex, while the pores of the material resulted in sensitive capacitance change under small pressure. Another recent example used three-dimensional (3D) microconformal graphene electrodes instead of the microstructured dielectric

[a] School of Textile Science and Engineering, Tiangong University, Tianjin 300387, China.
[b] School of Materials Science and Engineering, Tiangong University, Tianjin 300387, China.
[c] Institute for Frontier Materials, Deakin University, Geelong, Victoria 3216, Australia.
[d] Department of Chemistry, Biology, and Health Sciences, South Dakota School of Mines & Technology, Rapid City, South Dakota 57701, United States.
† Both authors contributed equally to the manuscript.
*Corresponding authors: wwy-322@126.com; zhengtao.zhu@sdsmt.edu
Electronic Supplementary Information (ESI) available: Schematic of sample preparation and device testing setup, characterization of PPy, stress-strain curves of the dielectric layer. See DOI: 10.1039/x0xx00000x

layer, resulting in a ultrasensitive flexible capacitive sensor with sensitivity of 7.68 $kPa^{-1}$ in a pressure range below 300 Pa.[7] Besides the conventional microfabrication and soft lithography techniques, innovative microstructure design strategies such as extrusion printing method,[33] laser microengineering,[34] rough substrate (e.g., sandpaper) molding,[35] and 3d printing[36] have been demonstrated as potentially low-cost alternative fabrication techniques of the microstructures for flexible pressure sensors.

While the capacitive sensors based on the microstructures offer highly sensitive response, they have limited pressure range. For the capacitive pressure sensors over a wide pressure range, spongy structures with high porosity and large pore size are designed as the dielectric layer.[37, 38] Highly porous Ecoflex dielectric layer with pore size ~300 μm and porosity ~ 60% was formed by using sugar cube as a template.[38] Capacitive pressure sensor based on such porous structure was capable of stable pressure sensing over the pressure range up to 130 kPa.[38] The detection range is largely determined by the porosity of the dielectric layer. However, high porosity of the dielectric layer may affect the mechanical stability, elasticity, reversibility, and hysteresis of the capacitive sensor.

The applications of the flexible capacitive pressure sensors in wearable technology are still limited by their detection range and sensitivity, high cost associated with preparation of microstructures, as well as the hysteresis of the dielectric materials. Herein, we report a flexible capacitive pressure sensor based on the dielectric PDMS elastomer with air gaps (through holes) and high porosity (denoted as agp-PDMS). Furthermore, the filter paper coated with polypyrrole (PPy) is used as a porous and rough electrode to make the contacts to the dielectric layer. The combination of pores/air gaps in the dielectric layer and the rough PPy electrode results in high sensitivity and stable pressure sensing over a wide pressure range. The porous and air gap PMDS elastomer is prepared by incorporation of sodium chloride (NaCl) powders and arrays of metal pins during the PDMS curing process. The rough contacts between the PPy electrode and the PDMS provide the sensitivity to the small deformation/pressure, while the highly porous PDMS layer responds dynamically to the high pressure of the large deformation. The sensor based on the air gaps/porous dielectric PDMS elastomer shows both high sensitivity and wide response range (up to 1 MPa). Applications in human motion monitoring are demonstrated using the prototype capacitive sensors and sensory array based on the air gaps/porous elastomeric dielectric material. Our results show that the combination of the porous PDMS dielectric layer and the PPy coated filter paper electrodes results in great improvement in the capacitive sensor detection range and sensitivity. Furthermore, incorporation of air gaps (i.e. through holes) in porous PMDS provide an effective way to increase the porosity while retain the mechanical strength of the dielectric layer, which may not be possible using only powders as template during the PDMS curing process.

## 2. Experimental Section

### 2.1 Materials

Polydimethylsiloxane (PDMS) and silicone elastomer curing agent were purchased from Dow Corning (Sylgard 184, USA). Ferric chloride ($FeCl_3$, 99.0%) was purchased from Tianjin Feng-Chuan Chemical Reagent Technologies Co., Ltd (China). Sodium chloride (NaCl, ≥99.5%) was purchased from Tianjin Jiang-Tian Chemical Technology Co., Ltd (China). Pyrrole (98%) was purchased from Sigma Aldrich Co., Ltd (Shanghai, China). All chemicals were used as received.

### 2.2 Preparation of the agp-PDMS dielectric layer

The process to prepare the agp-PDMS dielectric layer is illustrated in Fig. S1 (Supporting Information). To prepare the agp-PDMS layer, sodium chloride powders were used as a template. The 20.0 g NaCl granules were dissolved in 100 ml deionized water and recrystallized by evaporating water completely. The recrystallized NaCl crystals were ground to fine powders with a grinding crucible. The PDMS prepolymer (2.0 g) was mixed with the curing agent at a weight ratio of 10:1; then, the grinded NaCl powders (8.0 g) were added and mixed with the PDMS precursor. The PDMS precursor containing the NaCl powders was poured in a small glass container with dimension of 1 cm length × 1 cm width × 0.2 cm height. Subsequently, metal pins (e.g. 6 × 6 array) with diameter of 0.8 mm were inserted into the precursor mixture. The PDMS precursor with the NaCl powders and metal pins was cured in an oven at 150 °C for 15 min. After the pins were removed, the cured PDMS sheet was immersed in DI water to dissolve the NaCl powders. Finally, the PDMS sheet with pores and air gaps (i.e. agp-PDMS) was obtained after dried in air.

### 2.3 Preparation of the PPy/filter paper composite film

The PPy/filter paper composite film was prepared following Ref. 39. To deposit PPy on the filter paper, the filter paper was immersed in the 1.5 M $FeCl_3$ aqueous solution for 10 min and then sealed with the pyrrole vapor in a vacuum glass container for 12 h at room temperature. The PPy/filter paper composite film was rinsed with deionized water and dried in a vacuum oven at 60 °C for 1h.

### 2.4 Structural, morphology, and chemical characterization of agp-PDMS and PPy/filter paper composite sheet

The surface and cross-sectional morphologies of the agp-PDMS layer and the PPy/filter paper composite sheet were characterized by a Tabletop Microscope (Digital Microscope, TM-1000, Japan) and Field-Emission Scanning Electron Microscopy (FE-SEM, Zeiss Merlin Compact, German Zeiss Company, Germany). The porosity of the agp-PDMS was measured by a Mercury Porosimetry (Auto Pore IV 9510, Micromeritics Instrument Ltd., USA). The mechanical property of the agp-PDMS was characterized by Universal Testing Machine (INSTRON 5969, USA). The resistivity of the PPy/filter paper composite sheet was measured by ST2236-Double Testing Digital Four-Probe Tester (Suzhou Jingge Electronic Co., Ltd.). The chemical structures of the filter paper before and after PPy deposition were characterized by Fourier Transform Infrared Spectroscopy (FT-IR).

View Article Online
DOI: 10.1039/D0TC02477J





### 2.5 Preparation and characterization of the capacitive pressure sensor

The pressure sensor was prepared by using the PPy-filter paper composite film as the electrodes and the agp-PDMS as the dielectric layer, The agp-PDMS sheet with dimension of 1 cm length × 1 cm width × 0.2 cm thickness was sandwiched between two PPy-filter paper composite sheets. The PPy electrode was connected to the testing equipment using the copper adhesive tape. The sensor was packaged and fixed with transparent tape carefully on the testing apparatus to avoid pressure from the electric wires/connectors while retain good electric contacts between the device and the testing apparatus. Note that no adhesive was used between the dielectric layer and the PPy electrodes so there was only conformable van der Waals interaction between the layers.

A universal testing machine with a XC602-Stepping Motor Controller (Xinchang Electronics Technology Co., Ltd, Wuxi, China) was used to apply and measure the pressure on the sensor. The running speed of the stepping motor was 10 steps per second (0.033mm/s). A disk-type compression fixture with a diameter of 15 mm was in contact with the sensor to apply pressure uniformly. The force was recorded with a HP-100-Digital Force Gauge (Yueqing Aidebao Instrument Co., Ltd. Zhijiang, China), which had ± 0.5 % accuracy of the readout value with a force range of 0.1 - 100 N. When the force applied on the sensor was less than 0.1 N, scale weights were used**.** The capacitance of the sensor was measured with a precision LCR Meter (4090A, VICTOR, China) at a frequency of 10 kHz.

### 2.6 Demonstration of human motion detection and force mapping

To demonstrate monitoring of speaking, knee bending, and walking gait, a capacitive sensor based on agp-PDMS layer was attached to a volunteer's throat, knee, and sole of a foot, respectively. To maintain the stability of the sensor in different parts of a human body, the sensor was fixed with tape or elastic bandage. Change of capacitance was recorded with a digital multi meter during human motion. Informed consent from the volunteer was obtained for the experiment.

A sensor array with 3 × 3 pixels was fabricated by placing 9 pieces of agp-PDMS dielectric sheets embedded in the PPy-filter paper electrodes. Each electrode was extended by copper tape for wiring. The sensor array was packaged by a PDMS film. Three different weights were placed on the sensor array, and the capacitance changes of the 9 sensors were recorded. Similarly, one capacitive sensor was attached to each finger, and the capacitance changes were used to map the forces when a volunteer held a beaker.

## 3. Results and Discussion

### 3.1 Sensing mechanism

For capacitive pressure sensor, the capacitance depends on the area of the overlapped electrodes (A), the relative dielectric constant of the dielectric material ($\varepsilon_r$), and the distance between the two electrodes (d), based on the capacitance of a generalized parallel-plate capacitor, $C=A\varepsilon_r\varepsilon_0/d$, in which $\varepsilon_0$ is the permittivity of air, and $\varepsilon_r$ is the permittivity of the dielectric layer. In a sensor based on the porous elastomer dielectric layer, closing of the pores with increased applied pressure changes both the geometry and the dielectric constant of the capacitor, resulting in the capacitance change. High porosity of the dielectric layer may be beneficial for wide detection range and high sensitivity of the sensor. Furthermore, design of a pressure sensitive contacts between the electrodes and the dielectric layer may be further improve the sensitivity of the capacitive sensor, particularly at the small pressure range. For example, highly sensitive capacitive sensors were demonstrated using the electrodes with conformal graphene microstructures and PDMS dielectric layer.[7] In our work, PPy coated filter papers are used as the rough electrodes for the capacitive sensor. As we will discuss later, the PPy-coated filter paper has good conductivity and flexibility. More importantly, the PPy coating retains the fibrous structures of the filter paper, which results in rough contact surface and subsequently higher device sensitivity than copper electrode.

This work presents a flexible capacitive sensor with high sensitivity and wide detection range using the combination of the dielectric layer with the pores/air gaps (or through holes) and the rough electrode contacts. The mechanism of such pressure sensor is schematically illustrated in Fig. 1. The response of the sensor under pressure can be divided into three stages. In the first stage, when a small force is applied to the sensor, the capacitance change depends largely on the contacts between the rough PPy electrodes and the dielectric layer, since the changes of the effective permittivity and dimensions of the dielectric layer are relatively small. In this stage, the pores and air gaps do not change much, and the response of the device can be attributed to the change of the contact area between the PPy electrodes and the PDMS dielectric layer (Fig. 1, Stage 1). In Stage 2, continuous increase of the pressure starts to squeeze the air gaps and the pores of the dielectric layer. The large thickness change ($\Delta d_2$) and continuously increased effective permittivity

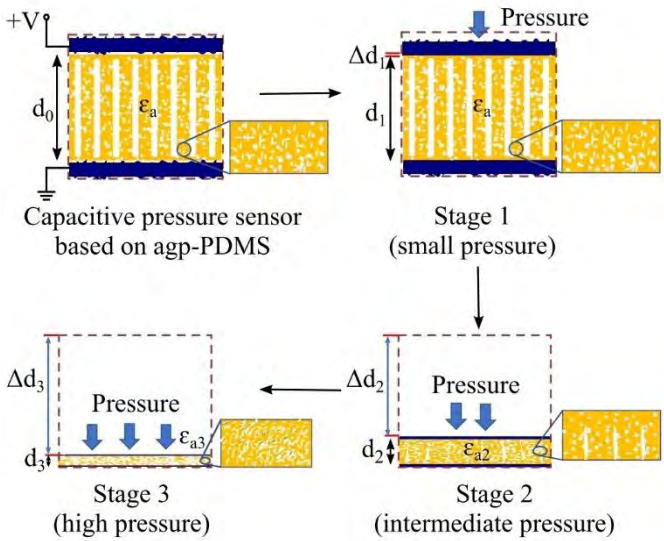


Fig. 1. Schematic of the mechanism of the capacitive sensor using porous and air gap elastomer as a dielectric layer.

View Article Online
DOI: 10.1039/D0TC04431





($\Delta\varepsilon_2$) result in significant capacitance change. At this stage, the effect of dimension change of the dielectric layer may dominate. While the air gaps and pores are squeezed significantly, some pores/air gap pockets would remain open in the dielectric layer. In Stage 3, under high pressure, the PDMS layer would be densified, and the dimension change would be small since most of the pores/air gap pockets would be closed. At this stage, the capacitance change is largely originated from the change of dielectric constant $\Delta\varepsilon_3$ with deformation of the remaining porous structure. Therefore, the capacitive sensor can maintain good sensitivity in the wide range of applied pressure. During the unloading process, the elastic restoring force of the elastomer allows reopening of closed pores and air gaps, and the agp-PDMS dielectric layer of the sensor returns to the initial state with good reversibility of the sensor response.

### 3.2 Characterization of the agp-PDMS dielectric layer and PPy-paper electrode

The capacitive pressure sensor consists of an agp-PDMS dielectric layer sandwiched between two flexible PPy/filter paper composite films, as schematically shown in Fig. 2a. The PPy/filter paper films served as the electrodes of the capacitive sensor, and the agp-PDMS sheet served as the dielectric layer. The capacitive sensor was packaged between two transparent tapes. The PPy/filter paper composite film was prepared by vapor polymerization of PPy. As shown in the two SEM images on the left of Fig. 2a, the PPy layer deposited on the filter paper formed continuous film on the fibers of the filter paper. The PPy/filter paper surface maintained the porous and fibrous morphology of the filter paper. The PPy particles had the diameters ranging from 185 to 285 nm with the average diameter of 228 nm (Fig. S2, Supporting Information). The average thickness over 10 different spots of the paper before and after pyrrole polymerization were measured. The average thickness of the filter paper and the PPy deposited filter paper was 0.188 mm and 0.266 mm, respectively. The surface resistivity of the PPy-filter paper composite film was 53.18 $\Omega/cm^2$, determined by the four-probe measurement. The FITR spectra of the PPy-filter paper composite (Fig. S3, Supporting Information) exhibited characteristic vibration modes of PPy with the C-N stretching vibration mode at 1470 $cm^{-1}$, the C-H in-plane mode at 1313 $cm^{-1}$ and out-of-plane mode at 1026 $cm^{-1}$, and the ring deformation mode at 906 $cm^{-1}$.[40, 41] The agp-PDMS sheet was first fabricated by using NaCl powders as a template. By using the NaCl powders as the template, highly porous PDMS was obtained, as shown in the two images on the right in Fig. 2a. The pore sizes of the porous PDMS ranged from 30 nm to 800 μm (Fig. S4, Supporting Information). The porosity of PDMS could be adjusted by using different amount of the NaCl powders during preparation. When the weight ratio of the NaCl powders to PDMS was 4 to 1, the porosity of the agp-PDMS sheet was 61.2% (denoted as PDMS-h); when the weight ratio of the NaCl powders to PDMS was changed to 2 to 1, the porosity of the agp-PDMS sheet was 30.4% (denoted as PDMS-l). PDMS-h and PDMS-l did not have air gaps.

The PDMS sheet with high porosity and air gaps was further prepared by using the NaCl to PDMS weight ratio of 4 to 1 and array of cylindrical pins. The diameter and the number of the air gaps (i.e. through holes) were determined by the cylindrical pins. Porous PDMS samples with arrays of 6 × 6, 4 × 4, 2 × 2 holes were created in the area of 1 $cm^2$; these samples were denoted as PDMS-h-$A_{66}$, PDMS-h-$A_{44}$ and PDMS-h-$A_{22}$, respectively. The diameter of the holes was ~850 μm, as shown in Fig. 2a. it is worth noting that besides 61.2% porosity created by the NaCl template, the PDMS-h-$A_{66}$, PDMS-h-$A_{44}$ and PDMS-h-$A_{22}$ samples had ~19.9%, ~8.9% and ~2.2% volume occupied by the air gaps, respectively. The compressibility and flexibility of the agp-PDMS elastomer, the PPy-filter-paper electrode, and the capacitance sensor, are shown pictorially in Fig. 2b. The stress-compressive strain responses of the prepared agp-PDMS dielectric materials are shown in Fig. 2c. Th response of pure PDMS sheet had a typical gradual linear region up to about 10% compressive strain followed by the rapid and nonlinear rising of stress with strain.[42] The porous agp-PDMS could deform much larger before the rapid increase of stress under compressive strain. In this case, the pores/air gaps in PDMS could collapse under relatively small applied pressure, resulting in small pressure change over a wide range of strain. The agp-PDMS became densified when the pores/air gaps were almost completely collapsed; and a rapid increase of the stress/pressure was observed as the compressive strain of the "densified" PDMS increased. As observed in Fig. 2c, the high porosity of pores/air gaps afforded high compressibility of the agp-PDMS materials. The compressive strain (78.33%) of the sample with highest porosity, PDMS-h-$A_{66}$, was 3.4 times larger than the strain (23.36%) of the solid PDMS sample under 1000 kPa pressure.

### 3.3 Sensor performance

Fig. S5a shows the scheme of the setup for the capacitive sensor characterization. The pressure applied on a device was controlled by a step motor, and the capacitance and pressure were measured by the LCR meter and the force gauge, respectively. The relative change of the capacitance is defined as $\Delta C/C_0$, in which $C_0$ is the capacitance of the sensor at zero pressure and $\Delta C$ equals the capacitance under pressure minus $C_0$. Fig. 3a shows $\Delta C/C_0$ as a function of the applied pressure (P) for the sensors based on the PDMS dielectric layers with different porosity. Evidently, changes of the capacitance $\Delta C/C_0$ using the porous dielectric layers were larger than that using the solid PDMS sheet as the dielectric layer. Moreover, $\Delta C/C_0$ of the device with the PDMS-h layer (i.e. the PDMS layer with 61.2% porosity) was larger than that of the sensor with PDMS-l layer (i.e. the PDMS layer with 30.4% porosity). The large change of $\Delta C/C_0$ could be attributed to the effect of the increased porosity on the mechanical and dielectric properties of the dielectric layer. As shown in Fig. 2c, with increase of the porosity, the strain increased at the same pressure. Additionally, the dielectric constant would decrease with increase of the porosity.[43] As a consequence, under the same pressure, the PDMS with high porosity would have large deformation and large change of dielectric constant, resulting in large capacitance change and improved sensitivity in the device with PDMS-h.[37, 38]

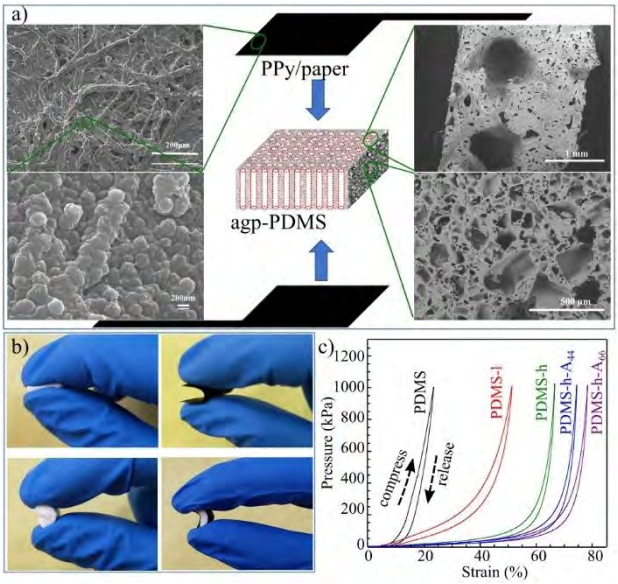


Fig. 2. (a) Schematic device structure of the flexible capacitive pressure sensor. The SEM images on the left showing the morphology of the PPy-filter paper nanocomposite film at different magnification; and the SEM images on the right showing the morphology of the top surface of the PDMS-h-$A_{66}$. (b) Photos showing the mechanical flexibility of PDMS-h-$A_{66}$ (two images on the left), the PPy-filter paper electrode layer (image at the upper right), and the assembled capacitive sensor (image at the lower right). (c) The pressure vs. compressive strain for PDMS, PDMS-l, PDMS-h, PDMS-$A_{44}$, and PDMS-$A_{66}$ samples.

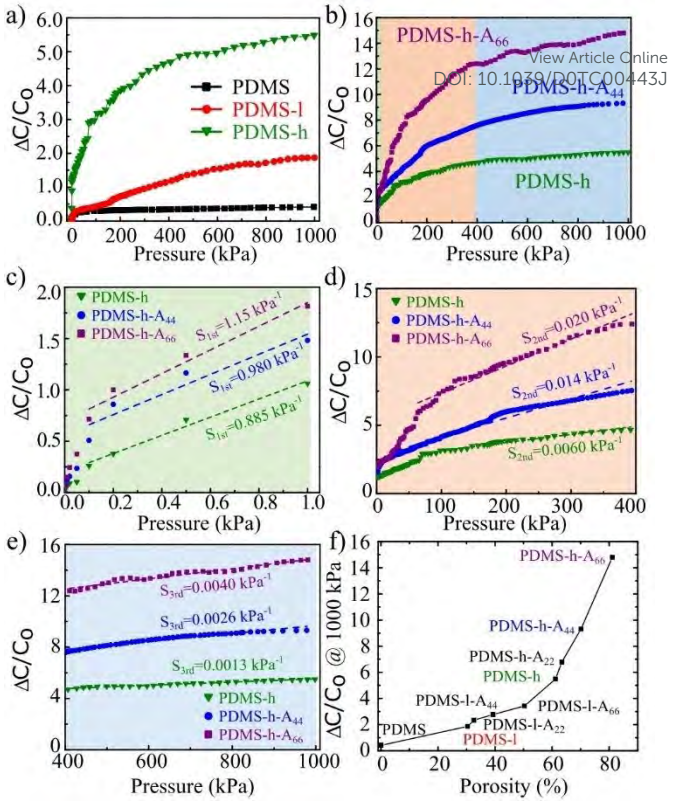


Fig. 3. (a) The relative capacitance change $\Delta C/C_0$ as a function of applied pressure for devices based on solid PDMS, PDMS-l,(30.4% porosity) and PDMS-h (61.2% porosity) (b) $\Delta C/C_0$ as a function of applied pressure for devices based on PDMS-h, PDMS-h-$A_{44}$(array of 4×4 holes), and PDMS-h-$A_{66}$ (array of 6×6 holes). The response of the devices under different pressure range is highlighted in different color. (c), (d), and (e) Enlarged plot of the $\Delta C/C_0$ as a function of applied pressure at small, intermediate, and large pressure ranges, respectively. The background colour corresponds to the pressure range highlighted in (b). (f) $\Delta C/C_0$ at 1000 kPa as a functional of the porosity of the dielectric layer.

To further improve the device performance, the PDMS sheets with high porosity and air gaps were used as dielectric layers. Fig. 3b compares $\Delta C/C_0$ under the applied pressure for the capacitive sensors with the PDMS-h, PDMS-h-$A_{44}$ and PDMS-h-$A_{66}$ layers. For clarity, the results of PDMS-h-$A_{22}$ were not included. In comparison with the performance of the porous PDMS-h, addition of air gaps in the PDMS-h-$A_{44}$ and PDMS-h-$A_{66}$ dielectric layers improved the $\Delta C/C_0$ response of the capacitive sensors over the wide range of pressure from 4.9 Pa to 1 MPa. The device based on the PDMS-h-$A_{66}$ dielectric layer had the largest changes of capacitance among the three devices. The sensitivity of the capacitive pressure sensor is defined as

$$S = \frac{\delta\left(\frac{\Delta C}{C_0}\right)}{\delta P},$$

in which P is the pressure, $\Delta C$ is the change of the capacitance, and $C_0$ is the capacitance under no applied pressure. Following the proposed mechanism in Fig. 1, the response and sensitivity of the capacitive sensors at stages of low, intermediate, and high pressures were presented in Fig. 3c, 3d, and 3e, respectively. At Stage 1, up to the pressure of ~1kPa (highlighted in green in Fig. 3b and enlarged in Fig. 3c), $\Delta C/C_0$ of the capacitive sensors increased rapidly with increase of the pressure. Besides the initial jump, $\Delta C/C_0$ could be fit linearly from 0.1 kPa to ~1 kPa, as shown in Fig. 3c. The sensor based on the PDMS-h-$A_{66}$ dielectric layer had the sensitivity of 1.15 $kPa^{-1}$, which was 1.18, and 1.30 times higher than those of the sensors based on the porous PDMS-h-$A_{44}$ (0.980$kPa^{-1}$), and the PDMS-h (0.885 $kPa^{-1}$) dielectric layers, respectively. The sensitivity of the sensor based on PDMS-h-$A_{66}$ in this low-pressure regime (<1 kPa) was relatively high in comparison to the sensors using various structures (e.g., the PDMS structure with tilted micropillar arrays (0.42 $kPa^{-1}$) [25] and the structure of nylon netting layers (0.33 $kPa^{-1}$)[26]). The high sensitivity of these agp-PDMS-based sensors under small pressure could be attributed to the deformation of the PPy/filter paper electrode and the change of the contacts at the electrode/dielectric interfaces.[7] As shown in Fig. S5b, the sensor based on PDMS-h-$A_{66}$ using the PPy/filter paper as electrodes was more than 2 times sensitive than the device using the copper electrodes. In addition to the contact effects of the rough PPy/filter paper electrode, the effective dielectric constant would increase as the pores were deformed with pressure. During compression, the air pockets in the pores ($\varepsilon_r$~1.0) would be squeezed out and replaced by the neighbouring PDMS material ($\varepsilon_r$~2.5). The highly porous structure and air gaps would also improve the compressibility of the dielectric layer, resulting in large change of strain (and thickness) under small stress (Fig. S6a, Supporting Information). These effects would be more pronounce in the dielectric layer with the large number of pores (i.e. PDMS-h-$A_{66}$ with ~60% porosity). It is worth noting that at this stage the deformation of the air gaps was presumably small, and the sensitivity would be largely determined by the contacts between PPy/filter paper electrodes and PMDS, thus a relatively small increase of sensitivity was observed with incorporation of air gaps.

At Stage 2, the intermediate pressure from ~1 to ~400 kPa, (highlighted in orange in Fig. 3b and enlarged in Fig. 3d), both the air gaps and pores would be compressed and deformed with increase of the pressure, and $\Delta C/C_0$ increased continuously because of the changes of the geometric and dielectric constant of the elastomer layer. As shown in Fig. S6b, the air gaps would improve the compressibility of the dielectric layer under intermediate pressure. In the range from 1 kPa to 400 kPa, a gradual decrease of sensitivity was observed; such change was common in the flexible capacitive sensors with further decrease of the pore volume and increase of the elastic resistance. As shown in Fig. 3d, the sensor response from ~100 kPa to 400 kPa would be fit linearly with sensitivities of 0.0060 $kPa^{-1}$, 0.014 $kPa^{-1}$ and 0.020 $kPa^{-1}$ for devices of PDMS-h, PDMS-h-$A_{44}$ and PDMS-h-$A_{66}$, respectively. At this intermediate pressure stage, the air gaps and pores in the dielectric layer would contribute synergistically to the change of capacitance, resulting in the higher $\Delta C/C_0$ and sensitivity of the devices based on PDMS-h-$A_{44}$ and PDMS-h-$A_{66}$ than the device with PDMS-h. The sensitivity of PDMS-h-$A_{66}$ was 3.4 times higher than that of PDMS-h, indicating the strong effect of air gaps on the device performance at this intermediate pressure range. The air gaps in PDMS might distribute most of the applied pressure, leaving certain number of pores remain open.

In Stage 3, when the pressure was up to 1 MPa (highlighted in blue in Fig. 3b and enlarged in Fig. 3e), changes of the capacitance were still observable even though most of the pores were closed under such high pressure. For the sensor based on PDMS-h-$A_{66}$, the sensitivity was 0.0040 $kPa^{-1}$ when pressure changed from 400 kPa to 1 MPa, which was more than 3 times higher than that of the device based on PDMS-h. The result indicated that the air gaps (i.e. through holes) improved the sensitivity of the sensor over a wide range of pressure, particularly for the high-pressure range. Such good sensitivity over the detection range up to 1 MPa was significant, in comparison to the sensitivities of the micropillar arrays-based sensor,[25] the microstructured porous pyramid-based sensor,[29] the wrinkled microstructures,[44] the bionic komochi konbu structure[45] based sensor, and the polymer foams-based sensor.[46] The good performance of the sensor based on PDMS-h-$A_{66}$ would be attributed to the air gaps of the material, which provided additional porous pockets under high pressure.

It is known that the detection range of the capacitive pressure sensor can be extended using the porous dielectric layer.[37, 38] However, the mechanical properties may be compromised when the porosity is too high. In our preparation of porous PDMS with the NaCl powders as the template, the PMDS-h reached the porosity of ~60%. To further increase the volume of pores (i.e. essentially the volume of the air pockets in the PDMS dielectric layer), different numbers of air gaps (i.e. through holes) with diameter of ~850 μm were generated by the metal pins along with the template PDMS preparation. The air gaps effectively increased the air pockets in the dielectric layer. The nominal "porosity" of the dielectric layer was calculated by adding the porosity generated by the NaCl template and the volume of the air gaps. The responses of the devices based on PDMS-l (30.4% porosity), PDMS-l-$A_{22}$ (30.4% porosity, array of 2×2 holes), PDMS-l-$A_{44}$ (30.4% porosity. array of 4×4 holes), PDMS-l-$A_{66}$ (30.4% porosity, array of 6×6 holes), and PDMS-h (61.2% porosity) were shown in Fig. S5c. In combination with the results of PDMS-h-$A_{22}$ (61.2% porosity, array of 2×2 holes), PDMS-h-$A_{44}$ (61.2% porosity. array of 4×4 holes), PDMS-h-$A_{66}$ (61.2% porosity, array of 6×6 holes), the $\Delta C/C_0$ of the sensors at 1000 kPa as a function of the porosity of the samples was plotted in Fig. 3f. The response of the device at high pressure increased exponentially with increase of the porosity. The result suggests that the air gap provide an effective way to increase the response of the capacitive sensor at high applied pressure range.

The capacitive sensor based on the PDMS-h-$A_{66}$ dielectric layer was selected for further studies of the sensor performance. Fig. 4a shows the relative capacitance change $\Delta C/C_0$ of the sensor under repeated loads of 2 g (196 Pa), 5 g (490 Pa), and 10 g (980 Pa) balance weights. Evidently, $\Delta C/C_0$ changed quickly and reversibly with loading and unloading of the weights, demonstrating that the capacitive sensor based on the air gaps/porous elastomeric dielectric layer had stable responses with high sensitivity and good reversibility. Response time and recovery time are important parameters of a capacitive pressure sensor. Fig. 4b shows the response and recovery time of the sensor based on PDMS-h-$A_{66}$ with loading and unloading of a 2 g balance weight. The capacitance of the sensor changed

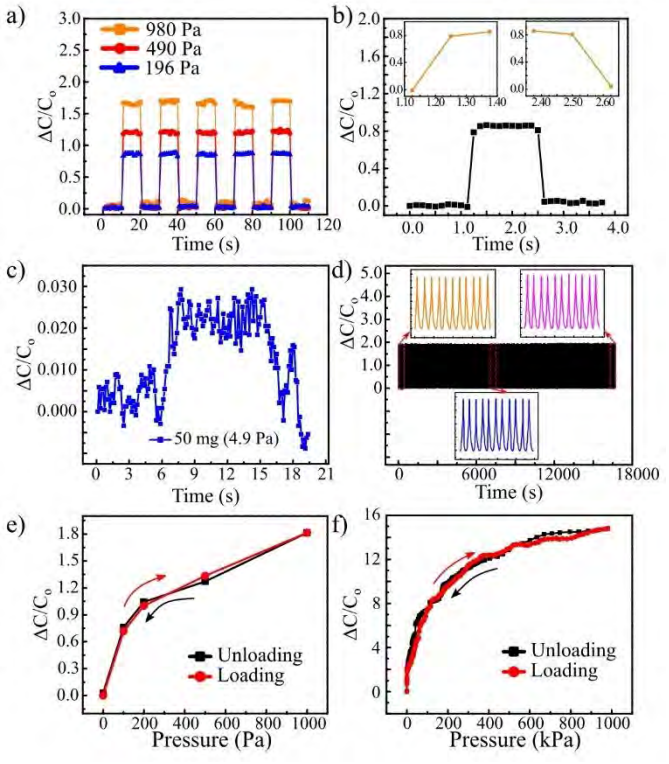


Fig. 4. (a) The dynamic response of $\Delta C/C_0$ for the device based on PDMS-h-$A_{66}$ under loading/unloading of balance weights of 2g, 5g, and 10g, corresponding to 196 Pa, 490 Pa, and 980 Pa, respectively. (b) Response and recovery time of the sensor based on PDMS-h-$A_{66}$ with loading and unloading of a weight of 2g. (c) the response of the sensor upon loading a weight of 0.0500g, corresponding to 4.9Pa. (d) $\Delta C/C_0$ of the sensor under over 1000 cycles of a repeated load/unload of pressure of 1.8kPa. (e) $\Delta C/C_0$ of the sensor as a function of applied pressure during loading and unloading pressure between 0 and 1000 Pa. (f) $\Delta C/C_0$ of the sensor as a function of applied pressure during loading and unloading pressure between 0-1MPa.

instantly upon weight loading, with a response time of 125 ms, as shown in the left inset of Fig. 4b. When the weight was removed, the capacitance of the sensor decreased with a fast recovery time of 125 ms (right inset of Fig. 4b). Note that the measurement of the response time was limited by the acquisition rate of the multimeter, so the actual response time of the device might be far less than 125 ms. Capacitive sensors are known to have quick response/recovery time.[19] Fig. 4c shows that the capacitive sensor based on PDMS-h-$A_{66}$ could sense the applied pressure as small as 4.9 Pa using a balance weight of 0.0500 g as the load. Note that the 4.9 Pa was approaching the limit of detection of the sensor so the response/recovery time could not be accurately determined. The stability of the sensor was evaluated by cycles of loading and unloading of ~1.8 kPa pressure linearly at a rate of 20 motor steps per second, controlled by a step motor. As shown in Fig. 4d, the sensor maintained a stable response of $\Delta C/C_0$ without deterioration for 1000 cycles (about 17000 s). The insets in Fig. 4d show the capacitance signals at different cycles of the measurement. The response of the device followed the applied pressure closely, and there was no obvious fatigue in the sensor performance during the 1000 cycles of loading and unloading, demonstrating the good durability of the capacitive sensor based on the air gap/porous PDMS dielectric material. Fig. 4e and 4f show the hysteresis of the air gaps/porous sensor under consecutive loading and unloading over a wide pressure range from 0-1000 kPa. The hysteresis of the sensor was negligible over the wide range of pressure. The hysteresis of our sensor was small than that of other flexible sensors with only micro-porous dielectric layer, such as the microporous PDMS dielectric layer by mixing PDMS and sugar,[46] and the porous spandex nanofiber webs dielectric layer by electrospinning technology.[47]

Various soft materials and novel strategies have been explored for skin-like capacitive sensors.[19] It is interesting to compare the performance of the flexible capacitive sensors in the literature with that of the device based on the rough PPy-filter paper electrode and the porous PDMS with air gaps, although such comparison is always challenging because of various device structures, device dimensions, testing range, and testing parameters. For the devices reported in this work, the PDMS-h-A66 (with a porosity of 61.2% + 6 × 6 holes))-based sensor performed the best. The sensitivity of the device was 1.15 $kPa^{-1}$ from ~5 Pa to 1.0 kPa, 0.020 $kPa^{-1}$ from 1.0 kPa to 400 kPa, and 0.0040 $kPa^{-1}$ from 400 kPa to 1 MPa. These values are on par or better than the recently reported porous PDMS based capacitive sensors[37, 38, 45, 48] in terms of the sensitivity and pressure range.

### 3.4 Applications of the capacitive pressure sensor in human motion monitoring

Various applications in human motion monitoring and force mapping were demonstrated using the flexible capacitive sensor based on the PDMS dielectric layer with air gaps and high porosity (i.e. PDMS-h-$A_{66}$). To demonstrate the detection of gentle motion, the sensor was attached to the throat of a volunteer using an elastic band. When the volunteer spoke the phonetic

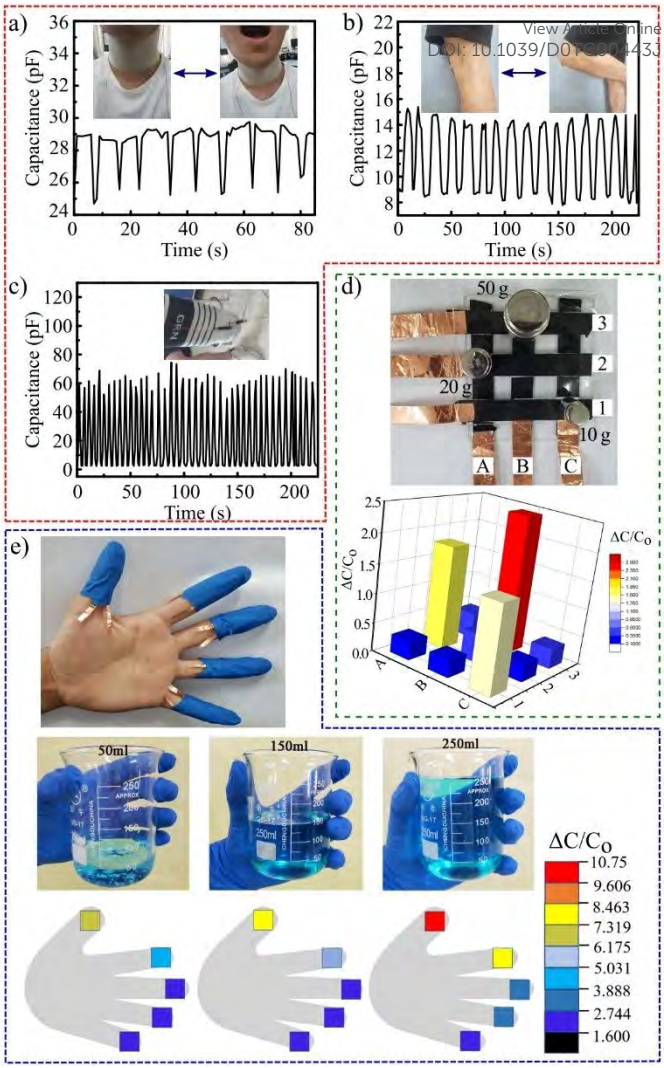


Fig. 5. Demonstration of the applications of the pressure sensor based on PDMS-h-A66 in monitoring of (a) speaking, (b) knee bending, and (c) walking. (d) Photo of a 3×3-pixel array of the capacitive sensor based on PDMS-h- A66 with three balance weights (top image) and the 3D ΔC/C0 mapping of the pressure distribution by the array of the capacitive sensors (bottom plot). (e) photo of the five capacitive sensors attached to the figures (top image), photos of holding beakers with different volumes of water by hand (middle images), and the corresponding force distribution on the five figures when holding beaker with water (bottom images).

alphabet "[ɑ:]" repeatedly, the change of the capacitance of the sensor was recorded. As shown in Fig. 5a and Movie S1, the capacitive pressure sensor based on PDMS-h-$A_{66}$ could detect the muscle movement associated with the sound with good repeatability. For detection of large body motion, the capacitive pressure sensor was attached on the knee of a volunteer. As shown in Fig. 5b and Movie S2, the capacitance of the sensor followed the movement of the knee; when the knee was bent, the capacitance increased; as the bend angle decreased, the capacitance decreased. In the third example, the capacitive pressure sensor was attached in the sole of a foot. As shown in Fig. 5c and Movie S3, the capacitive sensor detected the steps when the volunteer (weight 60 kg) walked normally. When the volunteer stepped on the floor, the value of the capacitance showed a rapid increase; and the capacitance value recovered quickly as long as the sole of the foot left the floor. The change of capacitance was much higher than those of speaking and knee

bending, in consistence with the much higher pressure of the walking motion. These results demonstrated that the flexible capacitive pressure sensor based on the porous and air-gapped elastomer dielectric layer could recognize the human motion over wide pressure range. Note that the different initial capacitance values of these results were originated from the ways these devices were interfaced and attached to different body parts. Tighter interface was needed to detect the subtle muscle motion of throat in Fig. 5a, whereas the sensor was readily attached to the foot sole in Fig. 5c.

Array of sensors can be used to monitor the spatial motion of an object, which is important for future development of human health monitoring and artificial intelligence. A prototype of array of 3×3 capacitive sensors based on PDMS-h-$A_{66}$ was demonstrated for force mapping. As shown in Fig. 5d, three balance weights of 10 g, 20 g and 50 g were placed at three locations tagged as 1C, 2A, and 3B, respectively. Evidently in the 3d Plot of $\Delta C/C_0$ of the sensor array, the capacitance changes of the array mapped the locations of the weights; the capacitance change was the largest at 3B, the second largest at 2A, and the smallest at 1C. $\Delta C/C_0$ values were 1.8, 2.4, and 1.5 at A2 (1.960 kPa), B3 (4.900 kPa), and C1 (980 Pa), respectively. The residue values at the other positions without load could be attributed to the possible crosstalk and interface between the array of capacitive devices. Such crosstalk and interface are known issues and may be addressed in future by using spacers to isolate the pressure sensitive capacitive devices.[14] To further demonstrate the capability of the capacitive sensors for monitoring complex motions, five sensors were placed at the tips of the fingers to detect the patterns of force loading when a volunteer grabbed a beaker with 50, 150, and 250 ml of water, as shown in Fig. 5e. The capacitance change of each sensor was recorded and labelled in the schematic of a hand. The result showed that the thumb and the index figure had the large force to hold the beaker, and the other three figures were used for fine adjustment. With increase of the weight of the beaker, the capacitance changes of the sensors increased, closely correlated to the increased forces needed to hold the beaker. From the capacitance change, the force of the figure applied to the beaker could be estimated. For example, $\Delta C/C_0$ of the thumb changed from 6.32 to 9.72 when the beaker changed from 50 ml to 250 ml; from these values, the pressure applied by the thumb on the beaker changed from ~75 kPa to ~210 kPa. These results demonstrated the potential application of the capacitive sensors in human motion monitoring.

## 4. Conclusions

In summary, a PDMS elastomer with high porosity and air gaps (through holes) was used as a dielectric layer for a flexible and highly sensitive capacitive pressure sensor over a wide detection range from ~5 Pa to 1 MPa. The high porosity of the PDMS elastomer and the rough PPy/filter paper conductive electrodes resulted in excellent capacitive sensor performance. The capacitive sensor had superior sensitivity (1.15 $kPa^{-1}$) for the pressure below 1 kPa. The sensor had the capability of detecting the applied pressure as small as 5 Pa. More importantly, the capacitive sensor based on the porous and air gap PDMS layer could measure the pressure over wide range up to 1 MPa. In the high pressure range from 400 kPa to 1 MPa, the sensor using PDMS with high porosity (61.2%) and air gaps had sensitivity as high as 0.0040 $kPa^{-1}$. These sensors had fast response/recovery time and stable response over 1000 cycles of pressure loading/unloading. Applications of the capacitive pressure sensors in human motion monitoring were successfully demonstrated (including speaking, joint bending, and walking). Additionally, array of sensors was fabricated to demonstrate spatial mapping of the pressure distribution. The excellent flexibility, high sensitivity, and wide pressure range of the capacitive pressure sensor based on highly porous and air gap elastomer dielectric layer demonstrated great potential applications in many fields.

## Conflicts of interest

There are no conflicts to declare.

## Acknowledgements

The research at Tiangong Univ. was supported by the National Science Foundation of China (51573136 and 51103101).

## Notes and references

1. W. Z. Li, L. Xiong, Y. M. Pu, Y. Quan and S. B. Li, *Nanoscale Res. Lett.*, 2019, **14**, 183.
2. Z. Wen, J. H. Yang, H. Z. Ding, W. L. Zhang, D. Wu, J. M. Xu, Z. F. Shi, T. T. Xu, Y. T. Tian and X. J. Li, *J. Mater. Sci.-Mater. Electron.*, 2018, **29**, 20978-20983.
3. X. Wang, Y. Gu, Z. Xiong, Z. Cui and T. Zhang, *Adv. Mater.*, 2014, **26**, 1336-1342.
4. P. Nie, R. Wang, X. Xu, Y. Cheng, X. Wang, L. Shi and J. Sun, *ACS Appl. Mater. Interfaces*, 2017, **9**, 14911-14919.
5. H. Qin, R. E. Owyeung, S. R. Sonkusale and M. J. Panzer, *J. Mater. Chem. C*, 2019, **7**, 601-608.
6. L. Ma, X. Shuai, Y. Hu, X. Liang, P. Zhu, R. Sun and C.-p. Wong, *J. Mater. Chem. C*, 2018, **6**, 13232-13240.
7. J. Yang, S. Luo, X. Zhou, J. Li, J. Fu, W. Yang and D. Wei, *ACS Appl. Mater. Interfaces*, 2019, **11**, 14997-15006.
8. M. Amit, R. K. Mishra, Q. Hoang, A. M. Galan, J. Wang and T. N. Ng, *Mater. Horizons*, 2019, **6**, 604-611.
9. Y. Lee, J. Park, S. Cho, Y.-E. Shin, H. Lee, J. Kim, J. Myoung, S. Cho, S. Kang, C. Baig and H. Ko, *ACS Nano*, 2018, **12**, 4045-4054.
10. C. Pang, G. Y. Lee, T. I. Kim, S. M. Kim, H. N. Kim, S. H. Ahn and K. Y. Suh, *Nat. Mater.*, 2012, **11**, 795-801.
11. G. Y. Bae, S. W. Pak, D. Kim, G. Lee, H. Kim do, Y. Chung and K. Cho, *Adv. Mater.*, 2016, **28**, 5300-5306.
12. K. Xia, C. Wang, M. Jian, Q. Wang and Y. Zhang, *Nano Res.*, 2018, **11**, 1124-1134.
13. Y. Wan, Z. Qiu, H. Ying, W. Yan, J. Zhang, Q. Liu, Z. Wu and C. F. Guo, *Adv. Electron. Mater.*, 2018, **4**, 1700586.
14. S. Pyo, J. Choi and J. Kim, *Adv. Electron. Mater.*, 2018, **4**, 1700427.
15. W. Y. Wang, Y. D. Zheng, X. Jin, Y. Sun, B. B. Lu, H. X. Wang, J. Fang, H. Shao and T. Lin, *Nano Energy*, 2019, **56**, 588-594.

16. H. Shao, J. Fang, H. Wang, C. Lang, G. Yan and T. Lin, *Macromol. Mater. Eng.*, 2017, **302**, 1600451.
17. X. He, Y. Zi, H. Yu, S. L. Zhang, J. Wang, W. Ding, H. Zou, W. Zhang, C. Lu and Z. L. Wang, *Nano Energy*, 2017, **39**, 328-336.
18. L. E. Helseth and X. D. Guo, *Sens. Actuator A Phys.*, 2016, **246**, 66-72.
19. S. Li, Y. Zhang, Y. Wang, K. Xia, Z. Yin, H. Wang, M. Zhang, X. Liang, H. Lu and M. Zhu, *InfoMat*, 2020, **2**, 184-211.
20. Y. Ding, T. Xu, O. Onyilagha, H. Fong and Z. Zhu, *ACS Appl. Mater. Interfaces*, 2019, **11**, 6685-6704.
21. X. Wang, L. Dong, H. Zhang, R. Yu, C. Pan and Z. L. Wang, *Adv. Sci.*, 2015, **2**, 1500169.
22. Y. Huang, X. Y. Fan, S. C. Chen and N. Zhao, *Adv. Funct. Mater.*, 2019, **29**, 1808509.
23. M. L. Hammock, C. Alex, T. Benjamin C-K, T. Jeffrey B-H and B. Zhenan, *Adv.Mater.*, 2013, **25**, 5997-6038.
24. J. A. Dobrzynska and M. A. M. Gijs, *Sens. Actuator A Phys.*, 2012, **173**, 127-135.
25. Y. Zhang, Y. Fang, J. Li, Q. Zhou, Y. Xiao, K. Zhang, B. Luo, J. Zhou and B. Hu, *ACS Appl. Mater. Interfaces*, 2017, **9**, 37493-37500.
26. B. C. Tee, A. Chortos, R. R. Dunn, G. Schwartz and Z. Bao, *Adv. Funct. Mater.*, 2014, **24**, 5427-5434.
27. S. C. B. Mannsfeld, Benjamin C-K, Tee, R. M. Stoltenberg, C. V. H. H. Chen, S. Barman, B. V. O. Muir, A. N. Sokolov, C. Reesee and Z. Bao, *Nat. Mater.*, 2010, **9**, 859-864.
28. Y. S. Luo, J. Y. Shao, S. R. Chen, X. L. Chen, H. M. Tian, X. M. Li, L. Wang, D. R. Wang and B. H. Lu, *ACS Appl. Mater. Interfaces*, 2019, **11**, 17796-17803.
29. Z. He, W. Chen, B. Liang, C. Liu, L. Yang, D. Lu, Z. Mo, H. Zhu, Z. Tang and X. Gui, *ACS Appl. Mater. Interfaces*, 2018, **10**, 12816-12823.
30. A. Chhetry, J. Kim, H. Yoon and J. Y. Park, *ACS Appl. Mater. Interfaces*, 2019, **11**, 3438-3449.
31. C. M. Boutry, A. Nguyen, Q. O. Lawal, A. Chortos, S. Rondeau-Gagne and Z. Bao, *Adv. Mater.*, 2015, **27**, 6954-6961.
32. J. C. Yang, J.-O. Kim, J. Oh, S. Y. Kwon, J. Y. Sim, D. W. Kim, H. B. Choi and S. Park, *ACS Appl. Mater. Interfaces*, 2019, **11**, 19472-19480.
33. Y. Gao, M. Xu, G. Yu, J. Tan and F. Xuan, *Sens. Actuator A Phys.*, 2019, **299**, 111625.
34. Y. Gao, C. Lu, Y. Guohui, J. Sha, J. Tan and F. Xuan, *Nanotech.*, 2019, **30**, 325502.
35. Y. Gao, G. Yu, J. Tan and F. Xuan, *Sens. Actuator A Phys.*, 2018, **280**, 205-209.
36. Y. Gao, G. Yu, T. Shu, Y. Chen, W. Yang, Y. Liu, J. Long, W. Xiong and F. Xuan, *Adv. Mater. Technol.*, 2019, **4**, 1900504.
37. S. Chen, B. Zhuo and X. Guo, *ACS Appl. Mater. Interfaces*, 2016, **8**, 20364-20370.
38. D. Kwon, T. I. Lee, J. Shim, S. Ryu, M. S. Kim, S. Kim, T. S. Kim and I. Park, *ACS Appl. Mater. Interfaces*, 2016, **8**, 16922-16931.
39. X. Zang, Y. Jiang, X. Wang, X. Wang, J. Ji and M. Xue, *Sens. Actuator B Chem.*, 2018, **273**, 1195-1201.
40. C. Yang, L. Zhang, N. Hu, Z. Yang, H. Wei and Y. Zhang, *J. Power Sources*, 2016, **302**, 39-45.
41. Y. Chen, K. Cai, C. Liu, H. Song and X. Yang, *Adv. Energy Mater.*, 2017, **7**, 1701247.
42. I. D. Johnston, D. K. McCluskey, C. K. L. Tan and M. C. Tracey, *J. Micromechan. Microeng.,* 2014, **24**, 035017.
43. X.-D. Liu, Z.-L. Hou, B.-X. Zhang, K.-T. Zhan, P. He, K.-L. Zhang and W.-L. Song, *Appl. Phys. Lett.*, 2016, **108**, 102902
44. X. Zeng, Z. Wang, H. Zhang, W. Yang, L. Xiang, Z. Zhao, L.-M. Peng and Y. Hu, *ACS Appl. Mater. Interfaces*, 2019, **11**, 21218-21226.
45. J. Wang, R. Suzuki, M. Shao, F. Gillot and S. Shiratori, *ACS Appl. Mater. Interfaces*, 2019, **11**, 11928-11935.
46. S. Bilent, T. H. N. Dinh, E. Martincic and P.-Y. Joubert, *Sensors*, 2019, **19**, 1968.
47. M. S. Reza, K. R. Ayag, M. K. Yoo, K. J. Kim and H. Kim, *Fiber. Polym.*, 2019, **20**, 337-347.
48. S. Kang, J. Lee, S. Lee, S. Kim, J. K. Kim, H. Algadi, S. Al-Sayari, D. E. Kim, D. Kim and T. Lee, *Adv. Electron. Mater.*, 2016, **2**, 1600356.

View Article Online
DOI: 10.1039/D0TC00443J

Table of Contents Entry

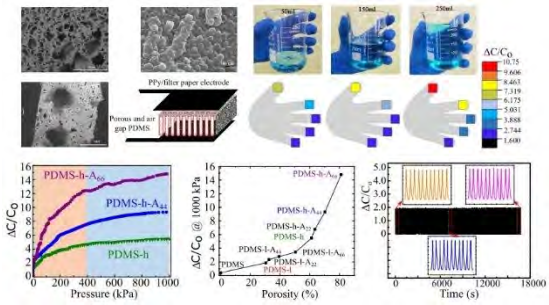


Capacitive sensor combining highly porous PDMS and rough polypyrrole electrodes improves the device range and sensitivity.